Climate mitigation averts corrosive acidification in the upper ocean

Sarah Schlunegger (sarah.schlunegger@princeton.edu)
Princeton University https://orcid.org/0000-0002-6668-9088

Keith Rodgers
Center for Climate Physics, INstitute for Basic Science https://orcid.org/0000-0002-6465-8923

Burke Hales
Oregon State University

John Dunne
Geophysical Fluid Dynamics Laboratory https://orcid.org/0000-0002-8794-0489

Masao Ishii
Meteorological Research Institute https://orcid.org/0000-0002-7328-4599

Ryohei Yamaguchi
Center for Climate Physics, Institute for Basic Science https://orcid.org/0000-0002-7800-5798

Richard Slater
Princeton University

Physical Sciences - Article

Keywords: anthropogenic carbon, marine science, ocean science

Posted Date: July 13th, 2021

DOI: https://doi.org/10.21203/rs.3.rs-648059/v1

Abstract

The invasion of anthropogenic carbon into the global ocean poses an existential threat to calcifying marine organisms[1–4]. Observations indicate that conditions corrosive to aragonite shells, unprecedented in the surface ocean, are already occurring in mesoscale upwelling features of the North Pacific[2,5,6] and Southern Ocean[7], and modeling experiments indicate that large volumes of the global ocean8 including the polar ocean's surface might become corrosive to aragonite by 2030[4,9–13]. Such changes are expected to compress important marine habitats, but the pathways by which habitat compression manifests over global scales, and their sensitivity to mitigation, remain unexplored. Using a suite of large ensemble projections from an Earth system model14,15, we assess the effectiveness of climate mitigation for averting habitat loss at the ecologically-critical horizon of the base of the ocean's euphotic zone. We find that without mitigation, 40-42% of this sensitive horizon experiences conditions corrosive to aragonite by 2100, with moderate mitigation this reduces to 16-19%, and with aggressive mitigation to 6-7%. Mitigation has a stronger effect on the eastern relative to western domains of the northern extratropical ocean with some of the greatest benefits in the ocean's most productive Large Marine Ecosystems, including the California Current and Gulf of Alaska. This work reveals the significant impact that mitigation efforts compatible with the Paris Agreement target of 1.5°C could have upon preserving marine habitats that are vulnerable to ocean acidification.

Main

Many scientific efforts towards understanding the sensitivity of marine calcifiers to ocean acidification have focused on the 'sentinel' Thecosomata pteropod, a pelagic zooplankton, also known as "sea butterflies" that form delicate shells of aragonite, a metastable mineral form of calcium carbonate. Pteropods are found throughout the global ocean [16] and play an important role in marine ecosystems and biogeochemical cycling. They consume phytoplankton in the ocean's euphotic zone[17], serve as an important food source for upper trophic levels including salmon and herring[17,18], and contribute significantly to regional sequestration of carbon at the ocean's surface via enhanced global export of carbon to depth [19–21].

Pteropods demonstrate acute sensitivity to the relative chemical availability (saturation) of aragonite in the local marine environment. Omega aragonite (Ω_{arag}), the saturation state of aragonite, expresses the favorability of sea-water for formation of aragonite. When Ω_{arag} is greater than unity ($\Omega_{arag} > 1$) , the formation of aragonite is favorable, when less than unity ($\Omega_{arag} < 1$) dissolution is favorable. Laboratory experiments and observations in the Southern Ocean and California Current suggest that brief exposure to low-Ω_{arag} waters, lasting only days to weeks, adversely impacts pteropod fitness and survival. Calcification rates slow when $\Omega_{arag} < 1.4$, and when $\Omega_{arag} < 1.0$ calcification ceases and habitat restriction is evident [7,22–24].

In this study we use projections from a suite of Initial Condition Large Ensemble simulations [25–27] of an Earth system model[14,15] (ESM; Supplementary Discussion 1 and Extended Data Figs. 1-2) to assess the benefits of climate mitigation efforts for reducing and delaying the progression of conditions corrosive to aragonite (i.e. $\Omega_{arag} < 1$). Pteropods vertically migrate about the seasonally-varying euphotic zone depth (EZD), feeding above the EZD during night and migrating below the EZD during day to escape visual predation[22]. We therefore evaluate Ω_{arag} at the EZD, thereby capturing the effects of the seasonal migratory patterns of our representative organism upon its vulnerability to ocean acidification (Methods, Extended Data Fig. 3). Using the Large Ensemble framework, we quantify the influence that internal climate variability has on the *onset* of aragonite undersaturation , the pace of *transition* between saturated and predominately undersaturated conditions [11], and on the robustness of mitigation efforts for curtailing aragonite undersaturation at the EZD.

Progression of aragonite undersaturation

We find undersaturated waters and associated habitat compression at the EZD are projected to progressively invade vast areas of the Arctic, Antarctic, subpolar gyres and equatorial upwelling regions by year 2050 (**Fig. 1a**). Under a high emissions scenario (RCP8.5), the affected regions expand between 2050 and 2100 to include the subtropical gyres of the North and South Pacific, the Eastern North Atlantic and the Equatorial Atlantic and Pacific. The transition period between the onset of month-long mean-state undersaturation and predominant undersaturation varies regionally from less than 5 years to more than 25 years (**Fig. 1b**). The transition period is significantly shorter in the Southern Ocean, North Atlantic and Subtropical North Pacific (<5 years) than in the Equatorial and Subpolar North Pacific (> 25 years, **Fig. 1b**). The influence of natural variability on the onset year of undersaturated conditions and length of the transition period is largest in the Atlantic and Pacific Eastern Boundary Currents and SubPolar North Pacific, where both the onset year and transition duration vary by over 25 years between ensemble members (**Fig. 1c**).

The spatial progression of undersaturated conditions (**Fig. 1a**) can be understood through the superposition of the historical or pre-industrial Ω_{arag} and the global invasion of anthropogenic carbon (C_{ant}; Extended Data Figs. 5-7). Regions where the mean-state historical saturation horizon (the depth at which $\Omega_{arag} = 1$) is already approaching the EZD, such as the Subpolar North Pacific and Eastern Boundary Upwelling Regions (Extended Data Fig. 6a) are susceptible to earlier onset of undersaturation events. Regions such as the Arctic and Southern Ocean, with already-low surface Ω_{arag} and weak vertical gradients in Ω_{arag} allow small additions of C_{ant} to drive large upward displacement of the undersaturation horizon and rapid transition to predominate undersaturation (**Fig. 1b**; Extended Data Figs. 5, 6b-c).

Impacts of mitigation on progression of undersaturation

Without mitigation efforts, undersaturated waters are projected to comprise 40-42% (range of ensemble members) of the EZD by 2100, representing potentially wide-spread habitat loss for aragonite calcifiers (**Fig. 2a**). However, saturation horizon shoaling is limited with moderate mitigation to the blue and green

regions (16-19%), and with aggressive mitigation, to the blue regions (6-7%). Moderate mitigation averts undersaturated conditions in the yellow regions, which include the subpolar and circumpolar, Arctic, equatorial, and eastern subtropical oceans. For the northern subpolar regions, the effects of mitigation are generally stronger in the east than west, reflecting the higher upper-ocean dissolved inorganic carbon (DIC) concentrations in the west (Extended Data Figs. 5,6). High DIC pre-conditions the west to more rapid undersaturation that outpaces mitigation benefits. The anthropogenic declines in Ω_{arag} and the sensitivity of these declines to mitigation is mediated by the magnitude of the invasion flux of C_{ant}, and not by anthropogenically-driven changes in circulation (Extended Data Fig. 7; Supplementary Discussion 2). This is important, as it suggests that our main results are not contingent on specifics of model sensitivity of the Atlantic Meridional Overturning Circulation (AMOC) stability but rather on the skill with which the model represents the upper ocean carbon cycle.

Mitigation also affords longer transition times in nearly all regions, but particularly in the Southern Ocean, where mitigation increases transition times from < 5 years on average to > 25 years (**Fig. 2c**). This reveals that in addition to reducing the spatial extent of habitat compression, aggressive mitigation also significantly increases the timescales available for migration [22], adaptation [28], and trophic adjustments to the reduction or local extinction of pteropods [29].

Many of the regions for which mitigation averts undersaturation are home to the world's Large Marine Ecosystem (LMEs), biogeographically defined provinces which cumulatively contribute 80% to the global fisheries yield [30] and contain the highest species richness and serve as biodiversity hotspots [31]. Mitigation more effectively averts aragonite undersaturation in LMEs located on the eastern side of the extra-tropical northern Pacific and Atlantic Oceans (**Fig. 3**). This contrast is exemplified in the North Pacific, where committed emissions ensure undersaturation by 2050 in the West Bering Sea and Oyashio Current whereas it is avoidable in the Gulf of Alaska and California Current.

Theoretical and empirical evidence suggest that compression of intermediate trophic levels, such as those occupied by pteropods, can result in deleterious effects at higher trophic levels [29]. The reduced abundance or absence of pteropods could have potentially large impacts on reliant species such as salmon and herring, and thus global fisheries [3]. Our results indicate that the timing of such impacts could differ by many decades between the eastern and western parts of each basin, and that near-term reductions in emissions will not mitigate the risk of undersaturation-related impacts in the western parts of the basins. This work motivates expansion of ongoing efforts to monitor plankton distributions and gut contents of key species as a key aspect of fisheries management for early warning of population vulnerability.

Impacts of vertical seasonal migration

The globally-integrated progression of one-month-per-year undersaturation is consistent across multiple depth horizons in the surface ocean (**Fig. 4**), with ~40% of each horizon experiencing month-long undersaturation events by year 2100 without mitigation, 20% with moderate mitigation and less than 10%

with aggressive mitigation. Despite the progression of onset being similar, the area impacted over the seasonal cycle is much less severe at the seasonally-varying EZD horizon (**Fig. 4a-c**) than at the fixed horizons (**Fig. 4e-f, 4i-k**). Differences in the expression of the seasonal cycle at the different horizons result in transition periods at the seasonally-varying EZD being longer (by more than 10 years on average) and more responsive to mitigation than at the 100 meters considered in previous studies [11,12] (**Fig. 4l**) or the annual-mean EZD (**Fig. 4h**).

During winter months, a shallower EZD offers a protectionary effect when the undersaturation horizon is also the shallowest in most regions (Extended Data Figs. 3b, 8). This protectionary effect of seasonal habitat movement delays the onset of predominant undersaturation therefore extending the transition period at the seasonally-varying EZD relative to the annual-mean EZD and 100-meter depth horizon (**Fig. 4d, 4h** and Extended Data Figs. 9-10), and consequently provides more leverage for mitigation efforts to increase transition durations. The distribution of transition times at the EZD reveals a stark contrast between the rapid transition period for RCP8.5, and successively longer adaptation timescales for RCP4.5 and then RCP2.6 (**Fig. 4d**), whereas the transition period defined at the annual-mean EZD and 100m depth for the three scenarios reveal nearly coincident peaks at less than 5 years (**Fig. 4h, 4l**).

Another critical difference between the progression of undersaturation at the EZD versus fixed-depth horizons is the time of year in which undersaturation begins to occur (Extended Data Fig. 10). At the seasonally-varying EZD, undersaturation arrives first in the summer months, whereas at 100 meters, undersaturation arrives first during winter months. This distinction may have important implications for spawning cycles and other seasonally-varying ecosystem drivers[3].

Conceptually, the length of the transition period is related to the ratio between the pace of anthropogenic-declines in Ω_{arag} and the amplitude of the seasonal cycle at a given static (100m) or dynamic (EZD) depth horizon (Extended Data Fig. 6d-i). The larger the amplitude of the seasonal cycle (or interannual variability in the case of Equatorial regions) in Ω_{arag} relative to anthropogenic declines in Ω_{arag}, the longer the transition period, i.e. more annual cycles are required for the majority of the year to fully surpass the undersaturation threshold. The amplitude of the seasonal and interannual variability in Ω_{arag} is also related to the vertical gradient in Ω_{arag}, with weak gradients producing weaker seasonal cycles (Extended Data Fig. 6c). Weak vertical gradients accelerate the transition, as the saturation horizon rapidly invades the euphotic zone. This mechanism gives insight into why transition periods differ: (*i*) between the EZD and fixed horizons (Extended Data Fig. 6g-i) – the anthropogenic declines in Ω_{arag} are similar but the amplitude of the Ω_{arag} seasonal cycle is larger when considered at the seasonally varying depth; (*ii*) across space – where the vertical gradient of Ω_{arag} varies by an order of magnitude between the poles and tropics (Extended Data Fig. 6b); and (*iii*) between different emissions scenarios, where mitigation reduces the rate of the anthropogenic declines in Ω_{arag} and therefore increases the transition period (**Fig. 4;** Extended Data Fig. 6g-i).

Discussion

Our findings extend the work presented in previous studies [11,12] by: (*i*) explicitly considering the impacts of mitigation on the progression of undersaturation, (*ii*) assessing undersaturation at the ecologically-motivated EZD rather than a fixed depth horizon, (*iii*) considering the global ocean and assessing risk and mitigation sensitivity across LMEs and (*iv*) identifying the fundamental importance of both the seasonal cycle in Ω_{arag} and EZD, as well as the vertical gradient of Ω_{arag}, in driving variations in transition times across regions. Our chosen threshold of strict undersaturation ($\Omega_{arag} < 1$) sustained for at-least a month represents a conservative estimate of when ocean acidification will begin to adversely and meaningfully impact pteropods. As such, the onset years presented here could understate the urgency of this ecological impact of climate change. Furthermore, other powerful changes in the ocean are underway, like warming and deoxygenation, which stand to interact and potentially exacerbate the pressures of acidification on pteropods and other marine calcifiers[32–34]. Additionally, the nominal 1° resolution of our ESM limits the representation of highly-localized variability (Supplementary Discussion 1), indicating that earlier localized undersaturation events may occur prior to the LME-to-biome scale undersaturation presented here.

The progression of acidification in the open ocean has relatively modest model uncertainty [35], and our analysis indicates that the rate at which aragonite undersaturation occurs in the upper ocean is largely driven by the superposition of the large-scale dynamics and the invasion flux of anthropogenic carbon (Extended Data Figs. 5-7), robust features of current generation ESMs unlikely to change meaningfully with improvements in model physics and resolution [36,37], however there are coastal and regional exceptions to model agreement [13,38], as well as model disagreement on the degree of amplification in seasonality of surface Ω_{arag} [39]. The Large Ensemble reveals that the onset and transition period of undersaturation are sensitive to natural variability uncertainty, shifting the timing by 25+ years over the Equatorial and the North Pacific. We find the spatial extent of this habitat compression is acutely sensitive to the magnitude of human emissions (e.g. large scenario uncertainty) and thereby displays a robust signature of mitigation efforts on reducing habitat loss (**Fig. 2**).

Our results emphatically present the potential of ocean acidification to vastly compress the habitable range of ecologically-, biogeochemically- and commercially-important taxa (**Fig. 1**). Habitat loss for pteropods in the ocean's polar regions is unavoidable given cumulative emissions to date. However, the extent to which habitat loss may be averted or stalled over the open ocean and in many highly productive LMEs throughout the Pacific, Atlantic, Indian and Southern Ocean is contingent on the degree to which aggressive emissions reductions are enacted (**Fig. 2**). Thus the degree of emission mitigation needed to avert substantial pteropod habitat compression, such as RCP2.6, is consistent with the goals of maintaining compliance with internationally recognized 1.5-2°C targets[40].

Methods

All simulations are conducted with the coupled Earth system model GFDL-ESM2M developed at the Geophysical Fluid Dynamics Laboratory [14,15] for which fidelity of the biogeochemical model (TOPAZ) has been documented for preindustrial [15] , historical [41] and future [42] boundary conditions. We also benchmark the performance of ESM2M's saturation state of aragonite (Ω_{arag}) during the contemporary period against data-based estimates. Specifically we assess ESM2M mean-state, anthropogenic trend and seasonal cycle relative to Ω_{arag} derived from ETHZ-OceanSoda [43], SOM-FFN [44], JMA-MLR [45] and for the Southern Ocean, the Biogeochemical Southern Ocean State Estimate [46] (B-SOSE). Model validation is discussed more fully in Supplementary Discussion 1.

We use a 30-member historical-forcing ensemble simulation (1950-2005) which then branches into 90 ensemble members for which 30 members are forced by a low-emission scenario (RCP2.6), 30 members are forced by a medium-emissions scenario (RCP4.5) and 30 members are forced by a high- or business-as-usual-emissions (RCP8.5) [47]. The initial conditions for the historical simulations are generated through using January 2nd-30th from year 1950 from the first ensemble member as the January 1st 1950 condition for ensemble members 2-30, constituting a micro-perturbation initialization procedure. The initial condition perturbations result in a rapid (within ~5 years) randomization of internal modes of variability across ensemble members. Initial conditions at year 2006 are taken from the historical ensemble, and each member is branched into a low-, medium- and high-emissions member, generating a total of 90 members of the 2006-2100 period. The initially-subtle differences in the forcing pathways between the 3 branched members re-introduces chaos such that members branched from the same historical ensemble member do not follow the same trajectory of internal variability after initialization. The historical and RCP8.5 simulations used here are distinct from those presented in the documentation papers[26,27], in that the 30 ensemble members used here include daily output of many fields and were conducted within a new computing structure which introduces differing round-off errors and thus internal-variability divergence relative to the original members. Nevertheless the statistics of natural variability, the mean state, and the sensitivity to climate perturbations are the same for the two sets of simulations.

New to this work is the analysis of Ω_{arag} at the time-varying base of the model's simulated Euphotic zone. Technically, this is done through saving the monthly mean three-dimensional Ω_{arag} and photosynthetically-active radiation (PAR) fields. We define the euphotic zone depth (EZD) as the model-calculated isoluminal horizon at which monthly-averaged PAR is equal to 0.1 Watts per square meter (Extended Data Fig. 3). The EZD exhibits seasonal variations driven by surface solar flux changes and ambient chlorophyll sustaining attenuation of light.

For each ensemble member, month, and each grid-cell, monthly-mean Ω_{arag} is then evaluated at the coincident euphotic zone depth. We define the ***onset*** of significant undersaturation as the first year which experiences a month of mean-state undersaturation. We define the ***transition*** period as the time between onset year, and the first year which experiences six months or more of mean-state undersaturation, i.e. the time it takes to transition from a permanently saturated to a predominately undersaturated mean-state. The onset and transition metrics are computed for each gridcell (re-gridded to 1°x1°). Where indicated, we

consider the fractional ocean area past onset within Large Marine Ecosystems (http://lme.edc.uri.edu/), with-in latitude bands and globally.

Additionally, in order to diagnose the difference between the radiative and chemical impact of rising atmospheric CO_2 on Ω_{arag}, we conduct a sensitivity experiment with ESM2M. The sensitivity experiment targeting attribution excludes the radiative impacts of rising atmospheric CO_2 on the climate system (i.e. no warming), while maintaining the carbon chemistry impacts of rising atmospheric CO_2 on air-sea gas exchange. This type of experiment can be referred to as biogeochemically-coupled or 'BGC'. *Concurrence* of the fully coupled Large Ensemble and the BGC experiment indicate the transient changes in the Large Ensemble arose from the chemical forcing of the invasion flux of anthropogenic CO_2. *Differences* between the fully coupled Large Ensemble and the BGC experiment indicate the transient changes in the Large Ensemble can be largely attributed to perturbations to the ocean and climate's physical state. As carbonate chemistry is non-linear, it is preferable to assess the impact of changes in ocean physics via its exclusion within an ocean of comparable carbonate-species concentrations to the fully-coupled Large Ensemble, hence why our experimental design includes the simulation with contemporary chemical forcing but pre-industrial radiative forcing. Pertinent results of these simulations and their comparison to the fully-coupled Large Ensemble are shown in Extended Data Fig. 7.

Declarations

Data availability

The Large Ensemble output used in this study is publicly available through Globus, with links and data-guide available at http://poseidon.princeton.edu.

Acknowledgments

Funding

S.S. acknowledges support by NSF's Southern Ocean Carbon and Climate Observations and Modeling (SOCCOM) Project under the NSF Award PLR-1425989, with additional support from NOAA and NASA. S.S. and K.B.R acknowledge support from NASA award NNX17AI75G, The work of K.B.R. and R.Y. were supported by the Institute for Basic Sciences (IBS), Republic of Korea, under IBS-R0278-D1. High Performance Computing resources were provided by NOAA Oceanic and Atmospheric Research/Geophysical Fluid Dynamics Laboratory.

Author contributions

S.S. and K.B.R conceptualized the study. S.S. performed all formal analysis. S.S. and K.B.R. wrote the initial text. S.S. and R.S. conducted the Large Ensemble experiments, with post-processing by K.B.R. M.I. assisted with selection and interpretation of data-based ocean acidification products. J. P. D. assisted with model validation. All authors contributed to the discussion and interpretation of the results.

Competing interests

The authors declare no competing interests.

Materials and Correspondence

The Large Ensemble output used in this study is publicly available through Globus, with links and data-guide available at http://poseidon.princeton.edu. Contact Sarah Schlunegger, sarah.schlunegger@princeton.edu, for additional information on and assistance using the GFDL Large Ensemble output.

References

1. Doney, S. C. *et al.* Climate change impacts on marine ecosystems. *Ann. Rev. Mar. Sci.* **4**, 11–37 (2012).
2. Feely, R. A. *et al.* Impact of anthropogenic CO2 on the CaCO3 system in the oceans. *Science* **305**, 362–366 (2004).
3. Bednaršek, N., Harvey, C. J., Kaplan, I. C., Feely, R. A. & Možina, J. Pteropods on the edge: Cumulative effects of ocean acidification, warming, and deoxygenation. *Prog. Oceanogr.* **145**, 1–24 (2016).
4. Orr, J. C. *et al.* Anthropogenic ocean acidification over the twenty-first century and its impact on calcifying organisms. *Nature* **437**, 681–686 (2005).
5. Bednaršek, N., Tarling, G. A., Bakker, D. C. E., Fielding, S. & Feely, R. A. Dissolution dominating calcification process in polar pteropods close to the point of aragonite undersaturation. *PLoS ONE* **9**, e109183 (2014).
6. Sutton, A. J. *et al.* Using present-day observations to detect when anthropogenic change forces surface ocean carbonate chemistry outside preindustrial bounds. *Biogeosciences* **13**, 5065–5083 (2016).
7. Bednaršek, N. *et al.* Extensive dissolution of live pteropods in the Southern Ocean. *Nature Geosci.* **5**, 881–885 (2012).
8. Gattuso, J. P. *et al.* OCEANOGRAPHY. Contrasting futures for ocean and society from different anthropogenic COâ emissions scenarios. *Science* **349**, aac4722 (2015).
9. Steinacher, M., Joos, F., Frölicher, T. L., Plattner, G. K. & Doney, S. C. Imminent ocean acidification in the Arctic projected with the NCAR global coupled carbon cycle-climate model. *Biogeosciences* **6**, 515–533 (2009).
10. Comeau, S., Gattuso, J.-P., Nisumaa, A.-M. & Orr, J. Impact of aragonite saturation state changes on migratory pteropods. *Proc. Biol. Sci.* **279**, 732–738 (2012).
11. Hauri, C., Friedrich, T. & Timmermann, A. Abrupt onset and prolongation of aragonite undersaturation events in the Southern Ocean. *Nat. Clim. Chang.* **6**, (2015).

12. Negrete-García, G., Lovenduski, N. S., Hauri, C., Krumhardt, K. M. & Lauvset, S. K. Sudden emergence of a shallow aragonite saturation horizon in the Southern Ocean. *Nat. Clim. Chang.* **9**, 313–317 (2019).
13. Terhaar, J., Kwiatkowski, L. & Bopp, L. Emergent constraint on Arctic Ocean acidification in the twenty-first century. *Nature* **582**, 379–383 (2020).
14. Dunne, J. P. *et al.* GFDL's ESM2 Global Coupled Climate–Carbon Earth System Models. Part I: Physical Formulation and Baseline Simulation Characteristics. *J. Clim.* **25**, 6646–6665 (2012).
15. Dunne, J. P. *et al.* GFDL's ESM2 Global Coupled Climate–Carbon Earth System Models. Part II: Carbon System Formulation and Baseline Simulation Characteristics*. *J. Clim.* **26**, 2247–2267 (2013).
16. Bednaršek, N., Možina, J., Vogt, M., O'Brien, C. & Tarling, G. A. The global distribution of pteropods and their contribution to carbonate and carbon biomass in the modern ocean. *Earth Syst. Sci. Data* **4**, 167–186 (2012).
17. Hunt, B. P. V. *et al.* Pteropods in Southern Ocean ecosystems. *Prog. Oceanogr.* **78**, 193–221 (2008).
18. Aydin, K. Y., McFarlane, G. A., King, J. R., Megrey, B. A. & Myers, K. W. Linking oceanic food webs to coastal production and growth rates of Pacific salmon (Oncorhynchus spp.), using models on three scales. *Deep Sea Res. Part II Top. Stud. Oceanogr* **52**, 757–780 (2005).
19. Berner, R. A. & Honjo, S. Pelagic sedimentation of aragonite: its geochemical significance. *Science* **211**, 940–942 (1981).
20. Acker, J. G. & Byrne, R. H. The influence of surface state and saturation state on the dissolution kinetics of biogenic aragonite in seawater. *Am. J. Sci.* **289**, 1098–1116 (1989).
21. Tréguer, P., Legendre, L., Rivkin, R. T., Ragueneau, O. & Dittert, N. Water Column Biogeochemistry below the Euphotic Zone. in *Ocean Biogeochemistry* (ed. Fasham, M. J. R.) 145–156 (Springer Berlin Heidelberg, 2003). doi:10.1007/978-3-642-55844-3_7.
22. Bednaršek, N. & Ohman, M. D. Changes in pteropod distributions and shell dissolution across a frontal system in the California Current System. *Mar. Ecol. Prog. Ser.* **523**, 93–103 (2015).
23. Bednaršek, N. *et al.* Exposure history determines pteropod vulnerability to ocean acidification along the US West Coast. *Sci. Rep.* **7**, 4526 (2017).
24. Bednaršek, N. *et al.* Systematic Review and Meta-Analysis Toward Synthesis of Thresholds of Ocean Acidification Impacts on Calcifying Pteropods and Interactions With Warming. *Front. Mar. Sci.* **6**, (2019).
25. Schlunegger, S. *et al.* Time of emergence and large ensemble intercomparison for ocean biogeochemical trends. *Global Biogeochem. Cycles* **34**, e2019GB006453 (2020).
26. Rodgers, K. B., Lin, J. & Frölicher, T. L. Emergence of multiple ocean ecosystem drivers in a large ensemble suite with an Earth system model. *Biogeosciences* **12**, 3301–3320 (2015).
27. Schlunegger, S. *et al.* Emergence of anthropogenic signals in the ocean carbon cycle. *Nat. Clim. Chang.* **9**, 719–725 (2019).

28. Peijnenburg, K. T. C. A. *et al.* The origin and diversification of pteropods precede past perturbations in the Earth's carbon cycle. *Proc Natl Acad Sci USA* **117**, 25609–25617 (2020).
29. Nagelkerken, I., Goldenberg, S. U., Ferreira, C. M., Ullah, H. & Connell, S. D. Trophic pyramids reorganize when food web architecture fails to adjust to ocean change. *Science* **369**, 829–832 (2020).
30. Pauly, D. *et al.* Fisheries in Large Marine Ecosystems: Descriptions and Diagnoses. *The UNEP Large Marine Ecosystem Report: a Perspective on Changing Conditions in LMEs of the World's Regional Seas* 23–40 (2008).
31. Tittensor, D. P. *et al.* Global patterns and predictors of marine biodiversity across taxa. *Nature* **466**, 1098–1101 (2010).
32. Lischka, S. & Riebesell, U. Synergistic effects of ocean acidification and warming on overwintering pteropods in the Arctic. *Glob Change Biol* **18**, 3517–3528 (2012).
33. Przeslawski, R., Byrne, M. & Mellin, C. A review and meta-analysis of the effects of multiple abiotic stressors on marine embryos and larvae. *Glob. Chang. Biol.* **21**, 2122–2140 (2015).
34. Gruber, N. Warming up, turning sour, losing breath: ocean biogeochemistry under global change. *Philos. Transact. A Math. Phys. Eng. Sci.* **369**, 1980–1996 (2011).
35. Frölicher, T. L., Rodgers, K. B., Stock, C. A. & Cheung, W. W. L. Sources of uncertainties in 21st century projections of potential ocean ecosystem stressors. *Global Biogeochem. Cycles* **30**, 1224–1243 (2016).
36. Arora, V. K. *et al.* Carbon–Concentration and Carbon–Climate Feedbacks in CMIP5 Earth System Models. *J. Clim.* **26**, 5289–5314 (2013).
37. Arora, V. K. *et al.* Carbon–concentration and carbon–climate feedbacks in CMIP6 models and their comparison to CMIP5 models. *Biogeosciences* **17**, 4173–4222 (2020).
38. Kwiatkowski, L. *et al.* Twenty-first century ocean warming, acidification, deoxygenation, and upper ocean nutrient decline from CMIP6 model projections. (2020) doi:10.5194/bg-2020-16.
39. Kwiatkowski, L. & Orr, J. C. Diverging seasonal extremes for ocean acidification during the twenty-first century. *Nat. Clim. Chang.* **8**, 141–145 (2018).
40. IPCC. Global warming of 1.5°C. An IPCC Special Report on the impacts of global warming of 1.5°C above pre-industrial levels and related global greenhouse gas emission pathways, in the context of strengthening the global response to the threat of climate change,. *Ipcc - Sr15* **2**, 17–20 (2019).
41. Frölicher, T. L. *et al.* Dominance of the southern ocean in anthropogenic carbon and heat uptake in CMIP5 models. *J. Clim.* **28**, 862–886 (2015).
42. Bopp, L. *et al.* Multiple stressors of ocean ecosystems in the 21st century: projections with CMIP5 models. *Biogeosciences* **10**, 6225–6245 (2013).
43. Gregor, L. & Gruber, N. OceanSODA-ETHZ: a global gridded data set of the surface ocean carbonate system for seasonal to decadal studies of ocean acidification. *Earth Syst. Sci. Data* **13**, 777–808 (2021).

44. Landschützer, P. *et al.* A neural network-based estimate of the seasonal to inter-annual variability of the Atlantic Ocean carbon sink. *Biogeosciences* **10**, 7793–7815 (2013).
45. Iida, Y. *et al.* Trends in pCO2 and sea–air CO2 flux over the global open oceans for the last two decades. *J. Oceanogr.* **71**, 637–661 (2015).
46. Verdy, A. & Mazloff, M. A data assimilating model for estimating Southern Ocean biogeochemistry. *Journal of Geophysical Research: Oceans* **122**, 1–22 (2017).
47. Moss, R. H. *et al.* The next generation of scenarios for climate change research and assessment. *Nature* **463**, 747–756 (2010).
48. Tabata, S. The general circulation of the Pacific Ocean and a brief account of the oceanographic structure of the North Pacific Ocean Part I - circulation and volume transports. *Atmosphere* **13**, 133–168 (1975).
49. Henson, S. A. *et al.* Detection of anthropogenic climate change in satellite records of ocean chlorophyll and productivity. *Biogeosciences* **7**, 621–640 (2010).

Figures

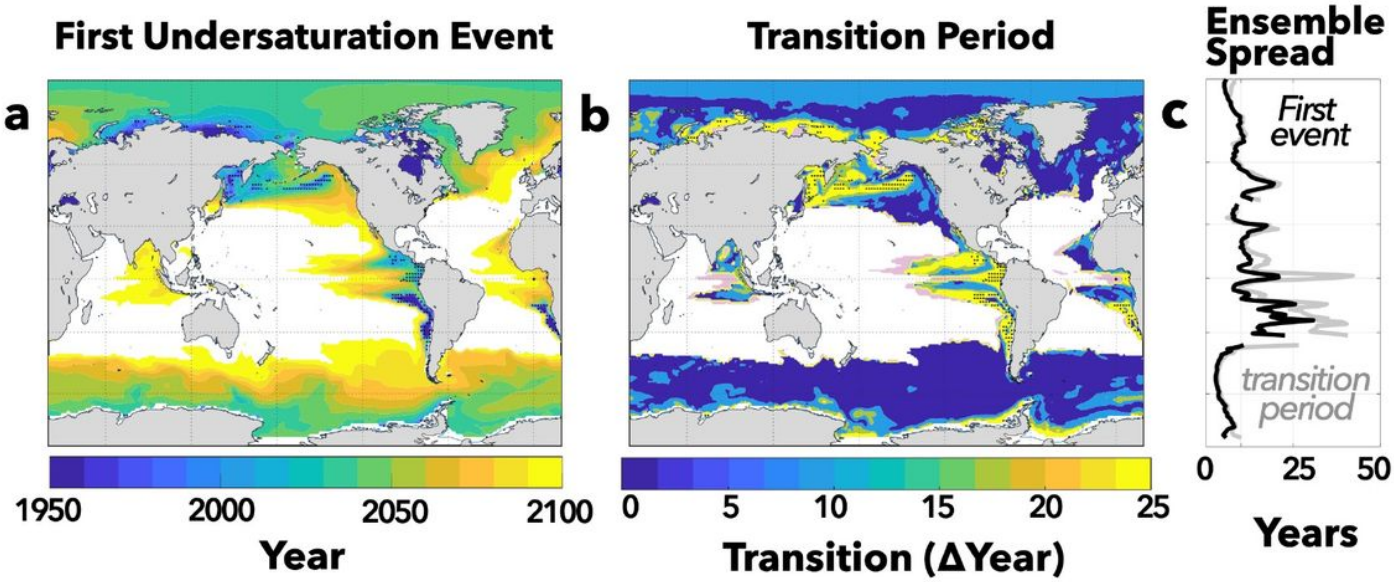

Figure 1

Timing of first exposure to month-long aragonite undersaturation and transition period between saturated and undersaturated states under RCP8.5 forcing (a) Expected time of first occurrence of undersaturation event at the EZD. (b) Expected transition timescale between the onset and the year at which 6 months or more is spent undersaturated (i.e. the annual cycle experiences predominate undersaturation). Pink shading indicates the grid-cell is not yet predominately saturated by 2100. (c) The zonal-mean ensemble range (impact of natural variability) in the onset (black) and the transition timescale (grey) where the range is the difference between the 10th and 90th percentile. Stippling in (a) and (b) indicates locations

where the 10th and 90th percentile ensemble members diverge by more than 25 years (Extended Data Fig. 4).

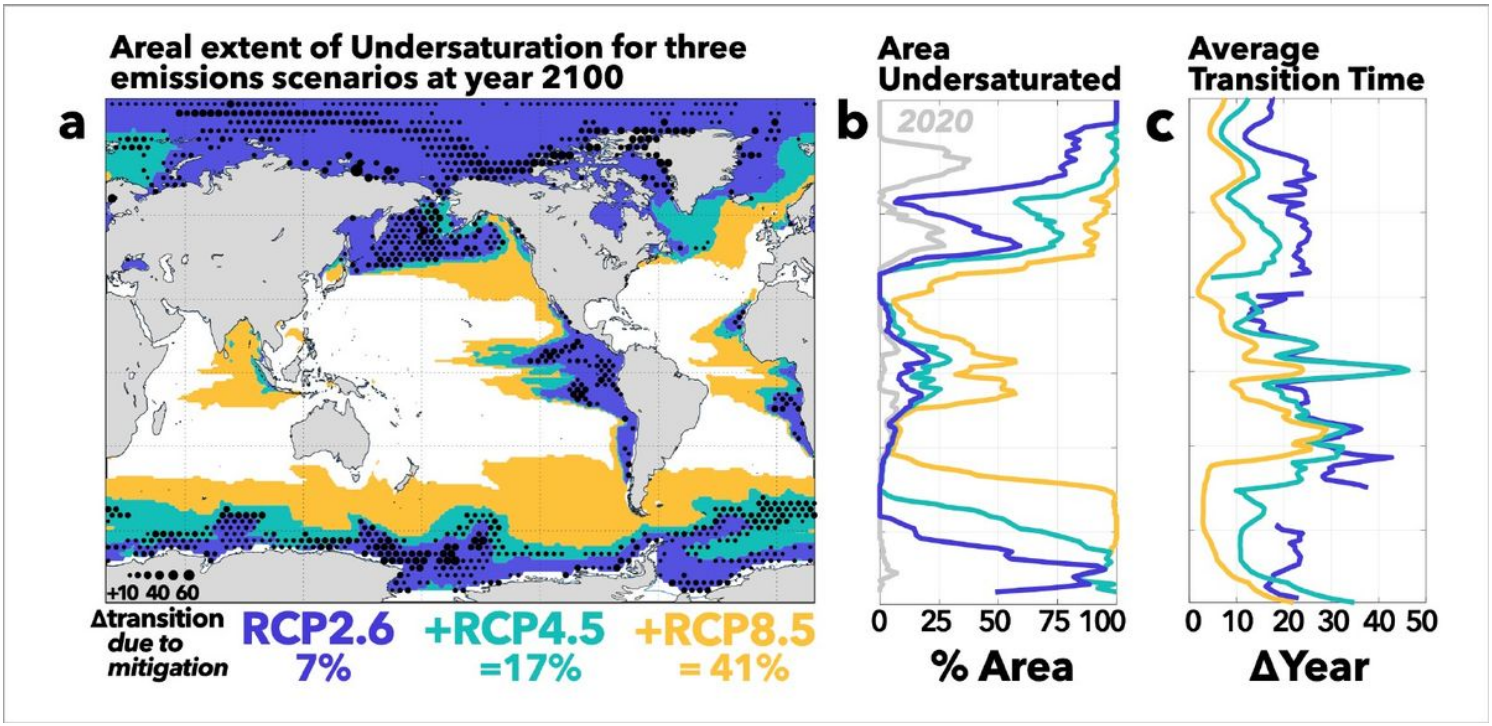

Figure 2

Impact of mitigation upon geographic extent of aragonite undersaturation and the transition time. (a) Extent of undersaturation under different emissions pathways at the EZD. The yellow area only experiences undersaturation under RCP8.5 forcing, i.e. undersaturation can be averted in the yellow regions with moderate mitigation (RCP4.5). Undersaturation in the green and yellow areas can be averted with aggressive mitigation efforts (RCP2.6). The blue area is where unavoidable “committed” undersaturation occurs by 2100. Stippling size indicates the length of extended transition period afforded by aggressive mitigation relative to business-as-usual. (b) The percent area of each latitude band that experiences undersaturation at year 2020 (grey) and by 2100 for the three emissions scenarios. (c) The average transition time between onset and a predominant undersaturation.

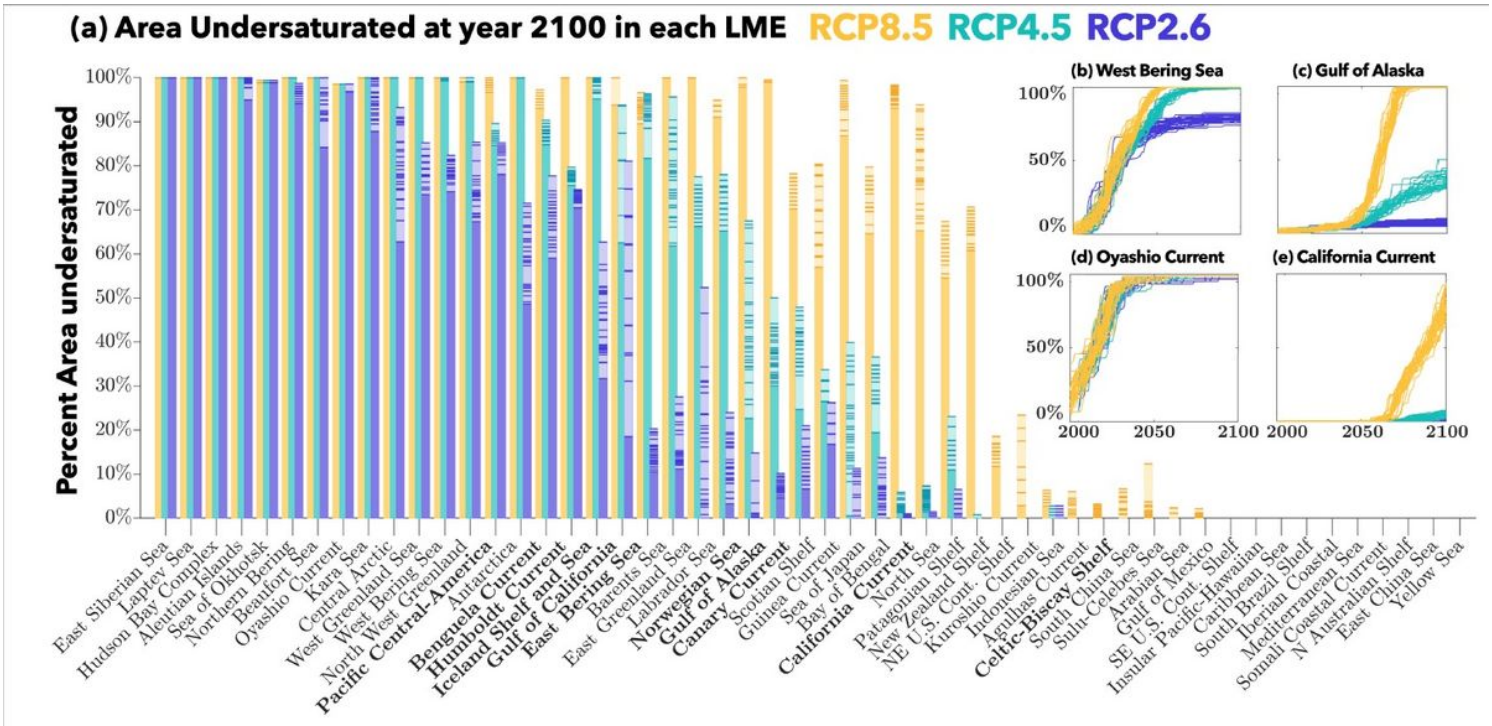

Figure 3

Area within each Large Marine Ecosystem which experiences aragonite undersaturation. (a) Percent area of each LME experiencing aragonite undersaturation at the EZD by 2100. Dark marks within each bar represent individual ensemble members and the spread of the ensemble is shaded lightly. Bold font indicates the region is in the Eastern sector of its basin, where mitigation efforts significantly reduce the impacted area. (b)-(e) Time-series plots of the percent area experiencing aragonite undersaturation in four selected LMEs in the North Pacific. For each scenario, all 30 ensemble members are plotted. LME domains given by http://lme.edc.uri.edu/.

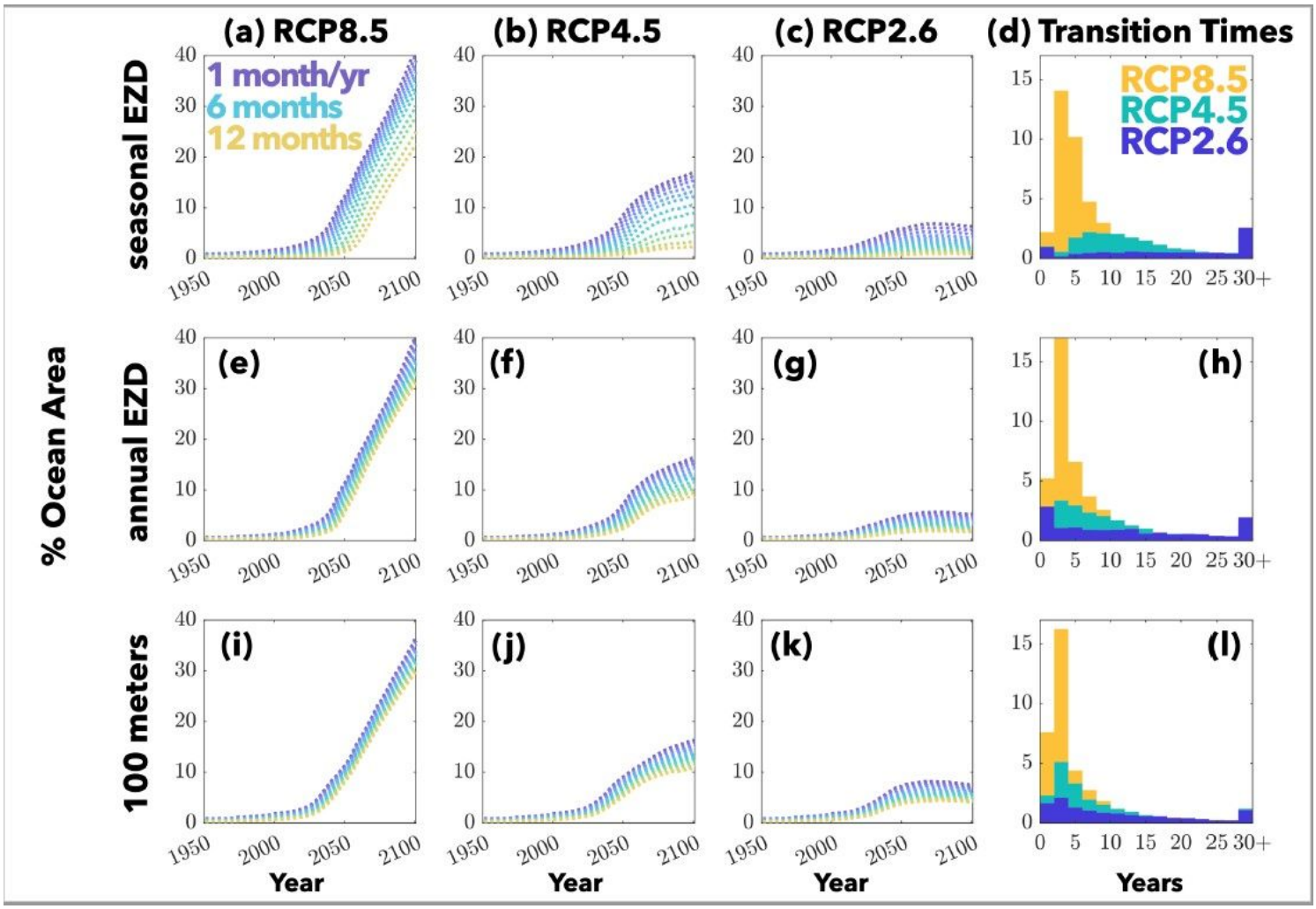

Figure 4

Ocean area experiencing aragonite undersaturation across the seasonal cycle at different depth horizons and the length and scenario-sensitivity of the transition period. Areal extent of undersaturated waters across the seasonal cycle (i.e. for the given number of months per year) for waters at the seasonally-varying EZD (a-c, top row), the annual mean EZD (e-g, middle row), and at 100 meters (i-k, bottom row). Panels (d,h,l) show distributions of transition duration in terms of percent area of ocean experiencing the given transition duration.

Supplementary Files

This is a list of supplementary files associated with this preprint. Click to download.

- SupplementaryInformation.pdf